KINEMATICS, WORKSPACES AND STIFFNESS OF A PLANAR CLASS-2 TENSEGRITY MECHANISM

Zhifei JI[1], Tuanjie LI[2], Min LIN[3]

In this paper, the kinematics, singular configurations, workspaces and stiffness of a planar class-2 tensegrity mechanism are studied. Firstly, the solutions to the kinematic problems are found by using a method of reduced coordinates. Then, the singular configurations are discussed and the workspaces are mapped. Afterwards, the stiffness of the mechanism is detailed with actuators locked. It is demonstrated that the stiffness is at a maximum when the mechanism is in equilibrium. Moreover, the stiffness always diminishes when subjected to external loads for the given actuator lengths.

Keywords: tensegrity; statics; kinematics; singularity analysis; stiffness;

List of symbols

ρ_1, ρ_2: Lengths of active prismatic actuators; L: Length of rigid rods
k_1, k_2, k_3, k_4: Spring constants; l_1, l_2, l_3, l_4: Current lengths of springs
x, y: Cartesian coordinates of node D; U: Potential energy of the system
J: Mechanism Jacobian; τ: External torque applied on node D
K: Stiffness of the mechanism

1. Introduction

The term tensegrity was created by Fuller [1] as a combination of the words tensional and integrity. It seems that he was inspired by some novel sculptures completed by Snelson [2]. The detailed history of tensegrity systems was reviewed by Motro [3]. Tensegrity systems are formed by a set of compressive components and tensile components. In this paper, we use the term rigid rods to represent compressive components and the term springs to represent tensile components. Tensegrity systems have advantages [4] of light-weight, deployability, easily tunable, etc. Due to these attractive characteristics, tensegrity systems have been used in several disciplines such as architecture, biology, aerospace, mechanics and robotics during the last fifty years [4].

The applications of tensegrity systems can be divided into two main branches. One application is used as structures and the other one is used as mechanisms. In addition, the research of tensegrity structures has two main issues, which are the form-finding problem and the behaviors under external loads. The form-finding of a tensegrity structure corresponds to the computation of the structure's

[1] Ph. D Candidate, School of Electro-Mechanical Engineering, Xidian University, CHINA.
E-mail: zfji18@163.com
[2] School of Electro-Mechanical Engineering, Xidian University, CHINA.
[3] School of Electro-Mechanical Engineering, Xidian University, CHINA.

equilibrium shape for a given set of parameters. This problem has been studied by many authors [5-7]. Moreover, a review of form-finding methods is given by Tibert [5]. The behaviors of tensegrity structures under external loads have also been researched by many researchers [8-9]. A static analysis of tensegrity structures was given by Juan and Tur [10].

When some components (rigid rods or springs) are actuated, tensegrity mechanisms can be obtained. In the past twenty years, several tensegrity mechanisms have been proposed [11-14]. The proposed applications of tensegrity mechanisms range from a flight simulator [15], a robot [16], and a space telescope [17] to a sensor [18]. During the past twenty years, considerable research has been performed on the control, statics and dynamics of class-1 tensegrity mechanisms. However, there are few articles relating to class-2 tensegrity mechanisms, especially on the study of them. The main objective of this article is to perform an analytical investigation of the kinematics and statics of a planar class-2 tensegrity mechanism. The definitions of class-1 and class-2 tensegrity systems are given by Skelton and Oliveira [4].

For conventional mechanisms, the kinematic analysis is often performed using geometric methods. Moreover, Staicu [19] developed a recursive matrix approach in kinematics modelling of serial mechanisms. However, for tensegrity mechanisms, the kinematics and statics of tensegrity mechanisms should be considered simultaneously [13]. Considering this characteristic, we used a method of reduced coordinates [20] to find the analytical solutions to the forward and inverse kinematic problems due to its convenient physical interpretation.

The use of springs as tensile components allows tensegrity mechanisms generate deformations with actuators locked. Several examples of the force-displacement relationships have been demonstrated numerically in [21-22]. However, the analytical relations between the external loads and the corresponding deformations of tensegrity systems were developed by using an energy method in [23]. The method was used in this paper to analyze the stiffness of the planar class-2 tensegrity mechanism.

2. Mechanism description

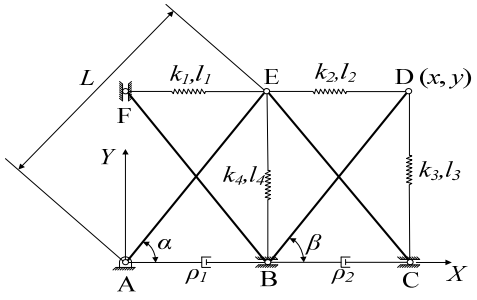

Fig. 1 Planar class-2 tensegrity mechanism

A diagram of the planar class-2 tensegrity mechanism is shown in Fig. 1. It consists of four compressive components and four tensile components. The compressive components are rigid rods joining node pairs AE, CE, BD and BF while the tensile components are springs joining node pairs EF, BE, DE and CD. The prismatic actuators are used to vary the distances between node pairs AB and BC.

From Fig. 1, it can be seen that node A is fixed to the ground. Nodes B and C are allowed to translate without friction along the X axis while node F is allowed to translate without friction along the Y axis. The angle between the X axis and the rigid rod joining nodes A and E is defined as α while the angle between the X axis and the rigid rod joining nodes B and D is defined as β. Moreover, the components are connected to each other at each node by 2-d rotational joints with frictionless and the whole mechanism lies in a horizontal plane. The rigid rods have the same length L. The actuator lengths, denoted by ρ_1 and ρ_2, are chosen as the mechanism's input variables while the Cartesian coordinates of node D, expressed by x and y, is chosen as the mechanism's output variables.

It is assumed that the springs are linear with k_i lengths l_i (i=1, 2, 3, 4) and zero free lengths. The last hypothesis is not problematic since, as was explained by Gosselin [24] and Shekarforoush et al. [25], virtual zero-free-length spring can be created by extending the actual spring beyond its attachment point. In this work, the Cartesian coordinates of nodes D and E are always chosen to be positive. For this reason, $0 \leq \alpha \leq \pi/2$, $0 \leq \beta \leq \pi$.

3. Kinematic analysis

For a tensegrity mechanism, the kinematics and statics of tensegrity mechanisms should be considered simultaneously [13]. For this reason, it is assumed that the mechanism considered here is always in an equilibrium configuration.

3.1 Forward kinematic analysis

The forward kinematic analysis of the mechanism studied here consists in computing the Cartesian coordinates of node D for the given actuator lengths ρ_1 and ρ_2. According to the method of reduced coordinates, the equilibrium configuration of the mechanism can be obtained by minimizing its potential energy with respect to a minimal number of parameters representing the shape of the mechanism. To obtain the potential energy of the mechanism, the coordinates of all nodes of the mechanism should be firstly computed.

As shown in Fig. 1, a cosine law for the triangle formed by nodes A, C and E can be written as follows.

$$\cos\alpha = \frac{\rho_1 + \rho_2}{2L} \tag{1}$$

Considering the range imposed to α, we obtain $\sin\alpha = \sqrt{1-\cos^2\alpha}$. Moreover, the coordinates of nodes B, C, D, E, and F can be computed as follows.

$$\begin{gathered}\mathbf{P}_{\mathrm{B}} = \begin{bmatrix}\rho_1 \\ 0\end{bmatrix},\ \mathbf{P}_{\mathrm{C}} = \begin{bmatrix}\rho_1 + \rho_2 \\ 0\end{bmatrix},\ \mathbf{P}_{\mathrm{D}} = \begin{bmatrix}\rho_1 + L\cos\beta \\ L\sin\beta\end{bmatrix} \\ \mathbf{P}_{\mathrm{E}} = \begin{bmatrix}L\cos\alpha \\ L\sin\alpha\end{bmatrix},\ \mathbf{P}_{\mathrm{F}} = \begin{bmatrix}0 \\ \sqrt{L^2-\rho_1^2}\end{bmatrix}\end{gathered} \tag{2}$$

The mechanism's configuration can be expressed as function of three independent parameters: two active variables ρ_1, ρ_1 and a redundant variable β.

Since the coordinates of node D are chosen as the output variables of the mechanism, we have

$$x = \rho_1 + L\cos\beta \tag{3}$$

$$y = L\sin\beta \tag{4}$$

With the coordinates of nodes B, C, D, E and F now known, the lengths of the four springs can be expressed as a function of ρ_1, ρ_2 and β. Therefore, the potential energy of the mechanism can be computed as follows.

$$\begin{gathered}U = \frac{2(k_1+k_2)+k_3+k_4}{2}L^2 + \frac{k_3\rho_2^2}{2} - \frac{k_1\rho_1^2}{2} - \frac{k_1\sqrt{(L^2-\rho_1^2)[4L^2-(\rho_1+\rho_2)^2]}}{2} - \\ \frac{\rho_1\rho_2(k_2+k_4)}{2} + \frac{k_2\rho_1-(2k_3+k_2)\rho_2}{2}L\cos\beta - \frac{\sqrt{4L^2-(\rho_1+\rho_2)^2}}{2}k_2L\sin\beta\end{gathered} \tag{5}$$

By differentiating the potential energy U with respect to the angle β and equating the result to zero, the following equation is generated.

$$\tan\beta = \frac{k_2\sqrt{4L^2-(\rho_1+\rho_2)^2}}{(2k_3+k_2)\rho_2 - k_2\rho_1} \tag{6}$$

Due to the range imposed to β, computing the arctangent of Eq. (6) generates a unique solution. Moreover, by substituting this result into Eqs. (3) and (4), a solution to the kinematic analysis is found. Especially, since the potential energy reaches its minimum when the mechanism is in equilibrium, the second derivative of U with respect to β is always positive.

3.2 Inverse kinematic analysis

The inverse kinematic analysis corresponds to the computation of the actuator lengths (ρ_1 and ρ_2) for the given Cartesian coordinates (x and y) of node D.

From Eqs. (3) and (4), the following equations can be derived.

$$(x-\rho_1)^2 + y^2 = L^2 \tag{7}$$

$$\tan\beta = \frac{y}{x-\rho_1} \tag{8}$$

Solving Eq. (7) for ρ_1 yields

$$\rho_1 = x + \delta_1\sqrt{L^2 - y^2} \tag{9}$$

where $\delta_1 = \pm 1$. Generally, when $0 \leq \beta \leq \pi/2$, $\delta_1 = -1$. When $\pi/2 \leq \beta \leq \pi$, $\delta_1 = 1$. By combining Eq. (6) with (8), the following equation is generated.

$$\lambda_2\rho_2^2 + \lambda_1\rho_2 + \lambda_0 = 0 \tag{10}$$

where

$$\lambda_0 = k_2^2\left[y^2\rho_1^2 - (x-\rho_1)^2\left(4L^2 - \rho_1^2\right)\right] \tag{11}$$

$$\lambda_1 = 2k_2\rho_1\left[k_2(x-\rho_1)^2 - (2k_3 + k_2)y^2\right] \tag{12}$$

$$\lambda_2 = y^2(2k_3 + k_2)^2 + k_2^2(x-\rho_1)^2 \tag{13}$$

Solving Eq. (10) for ρ_2, we obtain

$$\rho_2 = \frac{1}{2\lambda_2}\left[-\lambda_1 + \delta_2\sqrt{\lambda_1^2 - 4\lambda_2\lambda_0}\right] \tag{14}$$

where $\delta_2 = \pm 1$. From Eq. (14), two solutions for ρ_2 are obtained. Furthermore, considering the two solutions for ρ_1 given by Eq. (9), four solutions to the inverse kinematic analysis are found.

4. Singularity anlaysis

4.1. Mechanism Jacobian

For the mechanism considered here, the relationships between the input and output velocities can not be established since there are more degrees of freedom than actuators. However, because the mechanism is always assumed to be in equilibrium, its Jacobian, **J**, can be defined as follows.

$$\mathbf{J} = \frac{\delta\mathbf{v}}{\delta\boldsymbol{\psi}} = \begin{bmatrix} \dfrac{\partial x}{\partial\rho_1} & \dfrac{\partial x}{\partial\rho_2} \\ \dfrac{\partial y}{\partial\rho_1} & \dfrac{\partial y}{\partial\rho_2} \end{bmatrix} \tag{15}$$

where $\mathbf{v}=[x,\ y]^{\mathrm{T}}$ and $\boldsymbol{\psi}=[\rho_1,\ \rho_2]^{\mathrm{T}}$. Moreover, $\delta\mathbf{v}$ represents the infinitesimal changes of the mechanism's input variables while $\delta\boldsymbol{\psi}$ represents the infinitesimal changes of the mechanism's output variables. The elements of the Jacobian can be derived using Eqs. (3) and (4). As a consequence, the determinant of **J** can be obtained.

$$\det(\mathbf{J}) = \frac{2k_2L\cos^3\beta\left[\rho_1(k_2+k_3)(\rho_1+\rho_2) - 2L^2(2k_3+k_2)\right]}{\left[(2k_3+k_2)\rho_2 - k_2\rho_1\right]^2\sqrt{4L^2 - (\rho_1+\rho_2)^2}} \tag{16}$$

By examining the determinant of **J**, the singular configurations can be obtained. These singular configurations will be detailed in the following section.

4.2. Singular configurations

These singular configurations correspond to situations where the determinant of **J** is zero, goes to infinity or is indeterminate. With the elements of **J** computed from Eqs. (21)-(25), the determinant of **J** can be derived. By examining the Eq. (16), the expressions corresponding to singular configurations can be extracted. These expressions and the corresponding mechanism's behaviors are as follows.

i. $\cos\beta = 0$ and $\rho_2 \neq 0$

- The rigid rod joining nodes B and D is parallel to the Y axis.
- Finite movements of node D along the X axis are possible with the actuators locked.
- Infinitesimal movements of node D along the Y axis can not be generated.
- External forces applied at node D in a direction parallel to the Y axis can be resisted by the mechanism without generating any forces at the actuators.

ii. $4L^2 - (\rho_1 + \rho_2)^2 = 0$

- Node A is coincident with node F while node B is coincident with node E. In addition, node C is coincident with node D. Furthermore, all the nodes are located on the X axis.
- Infinitesimal movements of node D along the X axis can not be generated.
- Finite movements of node D along the Y axis are possible with actuators locked.
- External forces applied at node D in a direction parallel to the Y axis can not be resisted by the actuators. However, external forces applied at node D in a direction parallel to the X axis can be resisted by the mechanism without generating any forces at the actuators.

iii. $(2k_3 + k_2)\rho_2 - k_2\rho_1 = 0$ and $\rho_2 = 0$

- The nodes A, B and C are coincident with each other. All the mechanism's nodes are locked on the Y axis.
- Infinitesimal movements of node D along the Y axis can not be generated.
- Finite movements of node D along the X axis are possible with actuators locked.
- External forces applied at node D in a direction parallel to the X axis can not be resisted by the actuators. However, external forces applied at node D in a direction parallel to the Y axis can be resisted by the mechanism without generating any forces at the actuators.

From Fig. 1, it can be seen that the condition $0 \le \rho_1 \le L$ should be always satisfied. Especially, considering $0 \le \rho_1 \le L$ and $0 \le \rho_1 + \rho_2 \le 2L$, the following expression can be derived.

$$\rho_1 (k_2 + k_3)(\rho_1 + \rho_2) - 2L^2 (2k_3 + k_2) \le L \cdot (k_2 + k_3) \cdot 2L - 2L^2 (2k_3 + k_2) < 0 \qquad (17)$$

Therefore, the situation $\rho_1(k_2+k_3)(\rho_1+\rho_2)-2L^2(2k_3+k_2)=0$ does not correspond to any singular configuration. However, when $k_3 \to 0$, $\rho_1(k_2+k_3)(\rho_1+\rho_2)-2L^2(2k_3+k_2)=0$ corresponds to the singular point ($\rho_1=\rho_2=L$) in the actuator workspace.

5. Workspaces

5.1 Actuator workspace

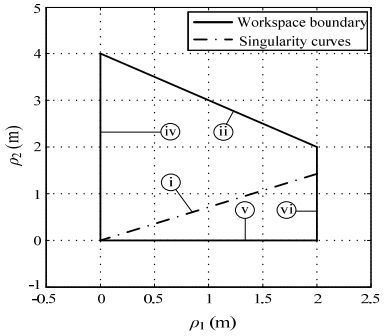

Fig. 2 Actuator workspace and singularity curves for a class-2 tensegrity mechanism with k_2=250 N/m, k_3=50 N/m and L=2 m.

For the mechanism, its actuator workspace is defined as the region that the actuators can reach. From section 4, it can be seen that each singular configuration is expressed in terms of the actuator lengths. As a consequence, the boundaries of the actuator workspace and the singular curves inside the actuator workspace can be mapped according to the singular configurations. An example of such a plot is shown in Fig. 2. In this figure, each curve is identified according to the singularity configurations listed in section 4 except curves iv, v and vi. From Fig. 1, it can be seen the prismatic actuator AB will reach its boundaries when $\rho_1=0$ or $\rho_1=L$. Therefore, the curves expressed by $\rho_1=0$ and $\rho_1=L$ correspond to the boundaries of the actuator workspace. From Fig. 2, it can be observed that curve iv corresponds to $\rho_1=0$ while curve vi corresponds to $\rho_1=L$. In Fig. 1, the range imposed to ρ_2 is $0 \le \rho_2 \le 2L-\rho_1$. Therefore, $\rho_2=0$ represent a part of the actuator workspace boundary to which curve v in Fig. 2 belongs. From Fig. 2, it should be noted that the singularity configuration described by item iii in section 4 corresponds to a point ($\rho_1=\rho_2=0$) of the actuator workspace boundary.

5.2 Cartesian workspace

The Cartesian workspace of the mechanism corresponds to the range of output variables. Since the actuator workspace of the mechanism was computed in section 5.1, the Cartesian workspace can be obtained by mapping the boundaries of the actuator workspace and the singular curves inside the actuator workspace into the Cartesian domain. An example of the mechanism's Cartesian workspace is shown in Fig. 3. The curves in Fig. 3 can be identified by the following expressions.

i $$y = L \tag{18}$$

ii $$y = 0 \tag{19}$$

iv $$x^2 + y^2 = L^2 \tag{20}$$

vi $$(x - L)^2 + y^2 = L^2 \tag{21}$$

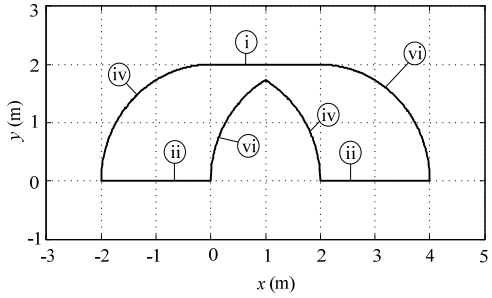

Fig. 3 Cartesian workspace for a class-2 tensegrity mechanism with k_2=250 N/m, k_3=50 N/m and L=2 m.

From Fig. 3, it can be seen that curves i and ii correspond to the singular configurations i and ii respectively. Moreover, curve iv corresponds to the situation ρ_1=0 while curve vi corresponds to the situation ρ_1=L. Especially, in the Cartesian domain, curves iv and vi can be described by Eqs. (20) and (21) respectively. In Fig. 3, it can also be observed that the singular curve i inside the actuator workspace corresponds to a part of the boundaries of the Cartesian workspace identified by curve i in the Cartesian domain. Furthermore, there are no singular curves inside the Cartesian workspace of the mechanism. This nature is attractive during the design of such mechanism.

6. Stiffness

From Fig. 1, it can be seen that the mechanism can generate deformation under the application of external loads with the actuators locked. The stiffness of a mechanism is defined as the ability to resist the deformation caused by external loads. An energy based method was used in [23] to develop the relationships

between the external loads and the corresponding deformations for a given tensegrity system. The method was employed in this work to evaluate the stiffness of the planar class-2 tensegrity mechanism.

When both actuators are locked, the only possible deformation of the mechanism is a rotation of the rigid rod joining node pairs B and D centered on node B. A relationship between an external torque applied to the rod BD and the corresponding deformation quantified by β can be found by differentiating U with respect to β (see Eq. (5)) as follows:

$$\tau = \left[\left(k_3 + \frac{k_2}{2}\right)\rho_2 - \frac{k_2}{2}\rho_1\right] L\sin\beta - \frac{k_2 L}{2}\sqrt{4L^2 - (\rho_1 + \rho_2)2}\cos\beta \tag{22}$$

where τ is defined as being positive when it tends to increase β. Moreover, the stiffness can be obtained as the slope of the torque profile.

$$K = \left[\left(k_3 + \frac{k_2}{2}\right)\rho_2 - \frac{k_2}{2}\rho_1\right] L\cos\beta + \frac{k_2 L}{2}\sqrt{4L^2 - (\rho_1 + \rho_2)2}\sin\beta \tag{23}$$

From Eqs. (5), (22) and (23), it can be seen that U, τ and K can be considered as functions of β. For the planar class-2 tensegrity mechanism, plots of U, τ and K as functions of β are shown in Figs. 6, 7 and 8, respectively with k_1=k_2=k_3=k_4=100 N/m, L=2 m, ρ_1=1 m and ρ_2=1.5 m. From Figs. 6 and 7, it can be seen that the potential energy U will reach its minimum when τ=0. Therefore, β_0 corresponds to the equilibrium configuration for the given actuator lengths. The condition $K \geq 0$ should be satisfied since the mechanism is always in a tensegrity configuration. Considering this condition, the maximum of β can be determined. As shown in Fig. 6, the maximum of β is identified by β_c.

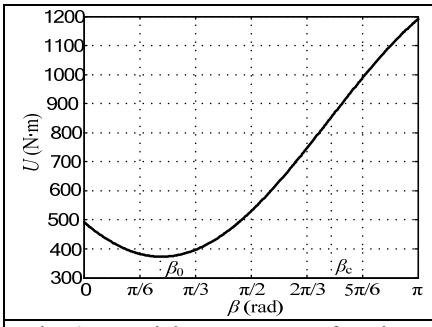

Fig. 4 Potential energy U as a function of β for the mechanism with k_1=k_2=k_3=k_4=100 N/m, L=2 m, ρ_1=1 m and ρ_2=1.5 m.

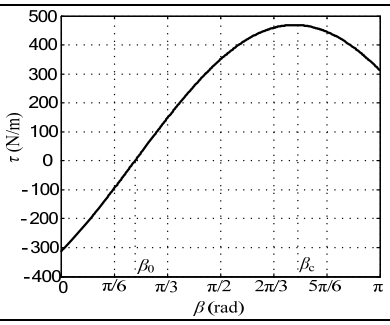

Fig. 5 Torque τ as a function of β for a class-2 tensegrity mechanism with k_1=k_2=k_3=k_4=100N/m L=2 m, ρ_1=1 m and ρ_2=1.5 m

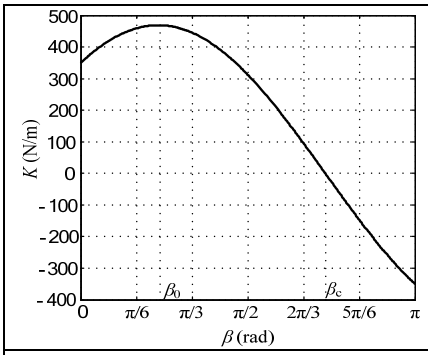

Fig. 6 Stiffness K as a function of β for a class-2 tensegrity mechanism with k_1=k_2=k_3=k_4=100 N/m, L=2 m, ρ_1=1 m and ρ_2=1.5 m.

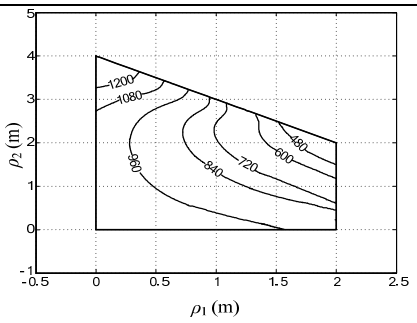

Fig. 7 Stiffness distribution in the actuator workspace for a class-2 tensegrity mechanism with k_2=250 N/m, k_3=50 N/m and L=2 m.

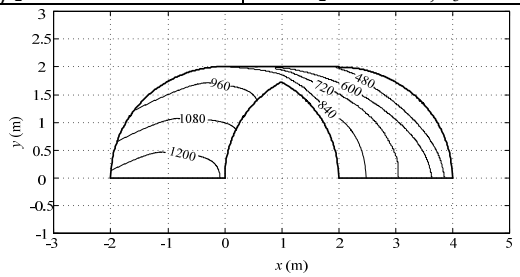

Fig. 8 Stiffness distribution in the Cartesian workspace for a class-2 tensegrity mechanism with k_2=250 N/m, k_3=50 N/m and L=2 m.

From Fig. 6, it can be observed that the stiffness K is at its maximum when the mechanism is in equilibrium and the stiffness decreases as the external torque increases. Furthermore, from Figs. 7 and 8, it can also be observed that the stiffness eventually becomes negative by increasing the external torque. The value of τ where K=0 is denoted τ_c. Should τ be increased slightly past τ_c and kept constant, the mechanism would collapse upon itself. From Figs. 6 and 7, it can be seen that the potential energy U increases with the external torque when $\beta < \beta_c$. However, when $\beta > \beta_c$, the external torque required to raise the potential energy of the mechanism is diminishing. Therefore, the mechanism will collapse upon itself when $\beta > \beta_c$.

When the mechanism is in equilibrium, it is necessary to analyze the distribution of the stiffness at equilibrium (τ=0) throughout the mechanism's workspaces. As mentioned in section 3, when the mechanism is in equilibrium, Eq. (6) can be obtained. Considering the range imposed to β, Eq. (6) gives a unique solution to β. By substituting this result into Eq. (23), the expression for K as a function of ρ_1 and ρ_2 can be obtained. Plot of K as a function of ρ_1 and ρ_2 is shown in Fig. 7. Fig. 7 illustrates the distribution of K in the actuator workspace. Furthermore, by plotting these distribution curves inside the actuator workspace

into the Cartesian domain, the distribution of K in the Cartesian workspace can be obtained as shown in Fig. 8. From Figs. 9 and 10, it can be seen that the stiffness varies considerably throughout the workspaces. This fact needs to be considered during the design and use of the mechanism.

7. Conclusion

An adaptive method of reduced coordinates was used in this paper to find the analytical solutions to the forward and inverse kinematic problems. According to the method of reduced coordinates, the equilibrium configurations can be obtained by minimizing the potential energy with respect to a minimal number of parameters representing the shape of the mechanism. Afterwards, the mechanism's Jacobian was computed. By examining the determinant of the Jacobian, the singular configurations were obtained. On the basis of the singular configurations, the actuator and Cartesian workspaces were mapped. It is revealed that there are no singular curves inside the Cartesian workspace. Then the relationship between the external load and the corresponding deformations was developed by an energy based method. As a consequence, the stiffness of the mechanism was evaluated. It was demonstrated that the stiffness is always at its maximum when the mechanism is in equilibrium. Furthermore, an increase in the external load leads to a decrease in the stiffness of the mechanism. Finally the stiffness distributions of the mechanism throughout its actuator and Cartesian workspaces were researched. Such stiffness distributions should be considered during the use of the mechanism.

Acknowledgment

This research is supported by the National Natural Science Foundation of China (No.51375360) and the Fundamental Research Funds for the Central Universities (No. K505131000087).

REFERENCES

[1] *B. Fuller*, Tensile-integrity structures, United States Patent No. 3063521, 1962.
[2] *K. Snelson*, Continuous tension, discontinuous compression structures, United States Patent No. 3169611, 1965.
[3] *R. Motro*, "Tensegrity systems: The state of the art", International Journal of Space Structures, **vol. 7**, no. 2, 1992, pp. 75-83.
[4] *R.E. Skelton and M.C. Oliveira*, Tensegrity Systems, Springer, New York, 2009.
[5] *A.G. Tibert and S. Pellegrino*, "Review of form-finding methods for tensegrity structures", International Journal of Space Structures, **vol. 18**, no. 4, 2003, pp. 209-223.
[6] *K. Koohestani*, "Form-finding of tensegrity structures via genetic algorithm", International Journal of Solids and Structures, **vol. 49**, no. 5, 2012, pp. 739-747.
[7] *H.C. Tran and J. Lee*, "Form-finding of tensegrity structures using double singular value decomposition", Engineering with Computers, **vol. 29**, no. 1, 2013, pp. 71-86.
[8] *N.B. Kahla and K. Kebiche*, "Nonlinear elasto-plastic analysis of tensegrity systems",

Engineering Structure **vol. 23**, 2000, pp. 1552-1556.
[9] *A. Nuhoglu and K. Korkmaz*, "A practical approach for nonlinear analysis of tensegrity systems". Engineering with computer, **vol. 27**, no. 4, Oct. 2010, pp. 337-345.
[10] *S.H. Juan and J.M.M Tur*, "Tensegrity frameworks: static analysis review", Mechanism and Machine Theory, **vol. 43**, no. 7, July 2008, pp. 859-881.
[11] *C.A. Mohr and M. Arsenault*, "Kinematic analysis of a translational 3-DOF tensegrity mechanism". Transactions of the Canadian Society for Mechanical Engineering, **vol. 35**, no. 4, 2011, pp. 573-584.
[12] *M.A. Swartz and, M.J.D. Hayes*, "Kinematic and dynamic analysis of a spatial one-DOF foldable tensegrity mechanism". Transactions of the Canadian Society for Mechanical Engineering, **vol. 31**, no. 4, 2007, pp. 421-431.
[13] *M. Arsenault and C.M. Gosselin*, "Kinematic and static analysis of a 3-PUPS spatial tensegrity mechanism". Mechanism and Machine Theory, **vol. 44**, no. 1, 2009, pp. 162-179.
[14] *M. Arsenault and C.M. Gosselin*, "Kinematic and dynamic analysis of a planar one-degree-of-freedom tensegrity mechanism", Journal of Mechanical Design, **vol. 127**, no. 6, 2005, pp. 1152-1160.
[15] *C. Sultan and M. Corless*, "Tensegrity flight simulator". Journal of Guidance, Control and Dynamics, **vol. 23**, no. 6, 2000, pp. 1055-1064.
[16] *C. Paul, F. J. Valero-Cuevas and H. Lipson*, "Design and control of tensegrity robots for locomotion. IEEE Transactions on Robotics", **vol. 22**, no. 5, 2006, pp. 944-957.
[17] *C. Sultan, M. Corless and R.E. Skelton*, Peak to peak control of an adaptive tensegrity space telescope, Proceedings of SPIE-The International Society for Optical Engineering (CSME) Forum, 1999, pp. 190-201.
[18] *C. Sultan and R. Skelton*, "A force and torque tensegrity sensor", Sensors and Actuators A: Physical, **vol. 112**, no. 2-3, 2004, pp. 220-231.
[19] *S. Staicu*, Methodes matricielles en cinématique des mecanismes, UPB Scientific Bulletin, Series D: Mechanical Engineering, **vol. 62**, no. 1, 2000, pp. 3-10.
[20] *C. Sultan, M. Corless and R.E. Skelton*, Reduced prestressability coordinates for tensegrity structures. Proceedings of the 40th AIAA/ASME/ASCE/AHS/ASC Structures, Structural Dynamics and Materials Conference, 1999, pp. 2300-2308.
[21] *C.D. Crane III, J. Duffy and J.C. Correa*, Static analysis of tensegrity structures Part 1: Equilibrium Equations. ASME 2002 International Design Engineering Technical Conferences and Computers and Information in Engineering Conference, 2002, pp. 671-680.
[22] *C.D. Crane III, J. Duffy and J.C. Correa*, Static analysis of tensegrity structures Part 2: numerical Examples, ASME 2002 International Design Engineering Technical Conferences and Computers and Information in Engineering Conference, 2002, pp. 681-687.
[23] *I.J. Oppenheim and W.O. Williams*, Geometric effects in an elastic tensegrity structure. Journal of Elasticity, **vol. 59**, no. 1-3, 2000, pp. 51-65.
[24] *C.M. Gosselin*, Static balancing of spherical 3-DOF parallel mechanisms and manipulators, The International Journal of Robotics Research, **vol. 18**, no. 2, 1999, pp. 819-829.
[25] *S.M.M. Shekarforoush, M. Eghtesad and M. Farid*, Design of statically balanced six-degree-of-freedom parallel mechanisms based on tensegrity system. 2009 ASME International Mechanical Engineering Congress and Exposition, 2009, pp. 245-253.